Naval Research Laboratory

Washington, DC 20375-5320

NRL/MR/6185--19-9904

Development of Spectroscopic Tools to Study Rarefied Gas Flows in Non-Equilibrium

Alfredo D. Tuesta
Brian T. Fisher

Navy Technology Center for Safety and Survivability
Chemistry Division

Logan T. Williams
Michael F. Osborn

Control Systems Branch
Spacecraft Engineering Department

December 31, 2019

REPORT DOCUMENTATION PAGE

Form Approved
OMB No. 0704-0188

1. REPORT DATE *(DD-MM-YYYY)*	**2. REPORT TYPE**	**3. DATES COVERED** *(From - To)*
31-12-2019	NRL Memorandum Report	03/11/2018 – 03/11/2019

4. TITLE AND SUBTITLE

Development of Spectroscopic Tools to Study Rarefied Gas Flows in Non-Equilibrium

5a. CONTRACT NUMBER

5b. GRANT NUMBER

5c. PROGRAM ELEMENT NUMBER
NISE

6. AUTHOR(S)

Alfredo D. Tuesta, Brian T. Fisher, Logan T. Williams, and Michael F. Osborn

5d. PROJECT NUMBER

5e. TASK NUMBER

5f. WORK UNIT NUMBER
N2P1

7. PERFORMING ORGANIZATION NAME(S) AND ADDRESS(ES)

Naval Research Laboratory
4555 Overlook Avenue, SW
Washington, DC 20375-5320

8. PERFORMING ORGANIZATION REPORT NUMBER

NRL/MR/6185--19-9904

9. SPONSORING / MONITORING AGENCY NAME(S) AND ADDRESS(ES)

Naval Research Laboratory
4555 Overlook Avenue, SW
Washington, DC 20375-5320

10. SPONSOR / MONITOR'S ACRONYM(S)

NRL NISE

11. SPONSOR / MONITOR'S REPORT NUMBER(S)

12. DISTRIBUTION / AVAILABILITY STATEMENT

DISTRIBUTION STATEMENT A: Approved for public release distribution is unlimited.

13. SUPPLEMENTARY NOTES

Karle Fellowship

14. ABSTRACT

Satellites, such as CubeSats, are used for a variety of educational and scientific purposes including surveillance, communication, and research. Their utility while in orbit can be greatly enhanced and prolonged by propulsion mechanisms such as micro-resistojets, which operate by expansion of gas through the nozzle. Although computer simulations have progressed in describing the high-speed viscous flow, experimental efforts are needed to validate and verify these models. Because of the low pressures (< 1 Torr) in which micro-resistojets operate and because of the high spatial resolution (100 um) required to resolve the nozzle exhaust at its exit diameter (1-2 mm), diagnostics of the micro-resistojet exhaust are difficult to achieve. To address this obstacle, a fiber-coupled, multiple-pass cell for spontaneous Raman scattering spectroscopy of the nozzle exhaust in a vacuum chamber was developed. Proof of principle measurements are successfully performed and illustrated at 1 Torr and 500 mTorr for H2 thermometry. Each spectral acquisition takes 15 and 30 minutes, respectively.

15. SUBJECT TERMS

Raman spectroscopy; Rayleigh spectroscopy; Multiple-pass cell; Low pressure spectroscopy; Non-equilibrium flow; Microjet; Resistojet

16. SECURITY CLASSIFICATION OF:			**17. LIMITATION OF ABSTRACT**	**18. NUMBER OF PAGES**	**19a. NAME OF RESPONSIBLE PERSON**
a. REPORT	**b. ABSTRACT**	**c. THIS PAGE**			Alfredo D. Tuesta
Unclassified Unlimited	Unclassified Unlimited	Unclassified Unlimited	Unclassified Unlimited	23	**19b. TELEPHONE NUMBER** *(include area code)* (202) 767-0803

Standard Form 298 (Rev. 8-98)
Prescribed by ANSI Std. Z39.18

This page intentionally left blank.

CONTENTS

INTRODUCTION **1**
REVIEW ON SCATTERING OF LIGHT **2**
LITERATURE REVIEW **2**
APPROACH **3**
Optical Design of Fiber Launch System **4**
Multiple-pass Cell **6**
Probe Volume **8**
Fitting Routine **8**
MEASUREMENTS IN GAS CELL **9**
Experimental Procedure **11**
RESULTS **11**
CONCLUSIONS **13**
FUTURE WORK **13**
ACKNOWLEDGEMENT **14**
REFERENCES **14**

FIGURES

Fig. 1-. 4
Fig. 2- 5
Fig. 3- 6
Fig. 4- 7
Fig. 5- 7
Fig. 6-. 8
Fig. 7- 10
Fig. 8- 10
Fig. 9- 11
Fig. 10- 12
Fig. 11- 12
Fig. 12- 13

TABLES

Tab. 1- 6

This page intentionally left blank.

DEVELOPMENT OF SPECTROSCOPIC TOOLS TO STUDY RAREFIED GAS FLOWS IN NON-EQUILIBRIUM

INTRODUCTION

The need for intelligence, surveillance and reconnaissance in the U.S. Navy is driving researchers to improve satellite technology and their propulsion systems in orbit. A particular type of satellite, known as a CubeSat, is widely used for scientific measurements and communication. They are relatively small, cubic in shape, and weigh only a few kilograms. As such, they are relatively inexpensive secondary payloads on greater launch endeavors.

CubeSats are excellent scientific tools performing various research objectives on the atmosphere and the planet while in orbit. However, they lack means to readjust their trajectory and, therefore, last only a few months before succumbing to the Earth's gravitational pull. In order to ameliorate this shortcoming and extend their lifespan, researchers are investigating the use of resistojets as propulsion mechanisms for these small satellites.

Resistojets are simple micro-jets that work by the expansion of gas through resistive heating in a chamber and the expulsion of the heated gas through a nozzle just 1 to 2 mm in diameter. Although simple in design, the thermodynamics, fluid dynamics, and heat transfer through the nozzle can be rather complex and difficult to model. In order to optimize various physical properties of the nozzle, a detailed understanding of the temperature, velocity and number density of the propellant gas is necessary.

The high-speed, viscous nature of the exhaust from the nozzle operating at low pressures yields a challenging environment for these studies. These conditions result in low number densities of the chemical species in the propellant and non-equilibrium of their internal modes. As such, techniques to investigate the rarefied gas must be sufficiently sensitive to function in the mTorr range and must have the capacity to discriminate between the internal and external modes of the molecules.

Raman and Rayleigh scattering spectroscopy are powerful diagnostic tools capable of investigating the non-equilibrium of the rotational, vibrational and translational modes of the gas molecules in the flow. The main challenge with these spectroscopic techniques, however, is the low signal in spontaneous Raman scattering (SRS) spectroscopy and the low spectral resolution in Rayleigh scattering spectroscopy. The signal in SRS spectroscopy is weak and proportional to pressure which, at the mTorr range, would be buried in electronic noise. Furthermore, the spectrum in Rayleigh scattering is weakly sensitive to changes in translational temperature and velocity, unresolvable by common spectroscopic instruments.

In this work, a novel multiple-pass cell approach will amplify the SRS signal and an innovative filtered Rayleigh scattering system will analyze the Rayleigh signal. Similar instruments with high spatial resolution have been developed for atmospheric flame experiments but currently do not exist for low-pressure measurements where non-equilibrium is most prominent. One of the essentials for the success of this work is the use of a continuous-wave laser rather than pulsed lasers, because the high fluence (W/cm^2) per pulse at low pressures would induce photo-dissociation in the molecules, perturbing and fundamentally changing the flow. These instruments will reveal the degree of non-equilibrium between the rotational, vibrational and translational temperatures, while also studying the bulk flow behavior namely velocity and number density.

Manuscript approved June 24, 2019.

REVIEW ON SCATTERING OF LIGHT

Light traveling through a gaseous medium predominantly scatters elastically, without exchanging energy with the molecules. This is known as Rayleigh scattering. However, a very small percentage of light interacts with the molecules and exchanges its energy. This can be detected by the change in frequency of the scattered light and is known as the Raman shift, usually measured in wavenumbers (1/cm). Discovered experimentally by C. V. Raman in 1928, the Raman effect refers to the small portion of light that scatters inelastically from molecules [1, 2].

Both, the elastic and inelastic scattering effects of light on molecules, is useful in spectroscopy to study the thermodynamic state of the molecules. In Rayleigh scattering, photons from a single frequency laser are Doppler shifted after scattering as a result of the thermal and bulk motion of the molecules. Also, the scattering intensity is proportional to the number density of the molecules. As such, Rayleigh spectroscopy can be used to examine the velocity, translational temperature, and concentration of molecules.

In spontaneous Raman scattering, the electromagnetic waves in light interact with the electron cloud of the molecules inducing a polarization. This polarization acts as a dipole on the molecule which oscillates at a resonant frequency defined by unique molecular parameters. The exchange in energy is quantized at the molecular level. Thus, inelastic light scattered can be shifted down or up in frequency depending on whether the quantum state of the molecule increases or decreases.

Because the quantized exchange is proportional to unique molecular parameters, the Raman shift detected in the spectrum of light scattered is a unique molecular fingerprint of the rotational and vibrational states of the molecules. The relative intensity of rotational transitions illustrated on a spectrum is a function of the rotational temperature of the molecule and modelled as a Boltzmann distribution, when in equilibrium [3]. The same is true for vibrational bands. As a result, Raman spectroscopy is an excellent technique to separately evaluate the internal modes of diatomic molecules in non-equilibrium [4, 5]. In some cases, the overall intensity of the spectrum can be calibrated to report a number density or concentration of the molecule [6].

In Rayleigh scattering, the elastic scattered light is at the same frequency as the incident laser light [7]. As a result, it can be difficult to discriminate between the source light and the scattered light. Using a filtered Rayleigh scattering approach, however, the center peak light in the Rayleigh spectrum can be attenuated so that the sidebands can be more closely inspected [8]. The intensity of the sidebands are proportional to the gas density and their shape, or width, is proportional to the translational temperature of the gas. Furthermore, due to the Doppler effect, spectral shifts in the Rayleigh signal are proportional to the velocity of the gas [9, 10].

LITERATURE REVIEW

The scattering of light has been used for decades to explore the thermodynamics of gaseous mediums. In combustion science, Raman scattering has been extensively used to explore the temperature of the flame and its chemical composition [11, 12, 13, 14, 15]. Often, temperature is derived from the spectrum of the N_2 vibrational bands and combustion relevant chemical species such as H_2, O_2 and CO_2 can be detected. Pulsed lasers can be used to deliver a dose of high beam fluence in a short period of time and in a relatively small probe region. In low pressure flows, however, the spontaneous Raman scattering signal is severely attenuated and a cavity-enhanced approach [16, 17, 18, 19] or multiple-pass cell [20, 21] are necessary.

Due to the unique spectral signature of each molecule, Raman spectroscopy is highly useful in monitoring multiple gases at once. Furthermore, the rotational and vibrational modes can sometimes be studied independently. This is particularly advantageous when examining nonequilibrium plasmas and supersonic shear layers [4, 22, 23, 24].

Rayleigh scattering has also been extensively used to explore gaseous flows [7]. In spite of the inability to spectroscopically distinguish between the light source and the scattered light, various techniques have been successfully developed and applied to study the translational temperature, gas density, and gas velocity. An atomic filter, such as an iodine cell has been used to attenuate the peak center intensity of the Rayleigh signal, thereby permitting analysis of the sidebands [8, 25]. A Rayleigh-Brillouin technique is particularly useful for remote sensing applications at a variety of temperatures and pressures [26, 27, 28]. Yet, another approach makes use of a Fabry-Perot interferometer to analyze the Rayleigh signal in flows at high sampling rates (kHz) [29, 30, 31, 32].

The small nozzle size of resistojets and their low-pressure flow make them difficult to study experimentally and model. To our knowledge, experimental efforts are far fewer than the theoretical models they attempt to validate. A non-linear, four-wave mixing version of Raman spectroscopy, known as coherent anti-Stokes Raman scattering (CARS) spectroscopy, has previously been used to study small nozzles and resistojets [33, 34]. CARS is capable of amplifying the Raman signal by directly inducing a polarization on the molecule. It is several orders of magnitude stronger in intensity than spontaneous Raman spectroscopy and can be highly spatially resolved. However, this approach is rather expensive and bulky, requiring at least two lasers and many optical components. Other experimental approaches have attempted to study the influence of nozzle geometry on thrust performance [35].

Modeling efforts, on the other hand, attempting to understand the high speed, viscous flow in small nozzles, have been more abundant [5, 33], especially from the US Air Force Research Laboratory [36, 37], NASA [38], and the US Naval Research Laboratory [39, 40]. They have highlighted the importance of the shear layer at the walls and the viscosity of the flow.

The objective of this work is to develop a diagnostic instrument, based on spontaneous Raman scattering spectroscopy and Rayleigh spectroscopy, capable of investigating the nonequilibrium flow of micro-nozzles. For this, the spectroscopic approach will have to provide highly spatially resolved measurements at low pressures which will offer a relatively compact and portable technique for these type of measurements.

APPROACH

By developing a highly spatially resolved spectroscopic instrument that significantly enhances the scattering signal of a low pressure gas in non-equilibrium, we can make use of spontaneous Raman scattering and filtered Rayleigh scattering to study the thermodynamics of the flow in a compact, cost-effective and fiber-coupled manner. There are other spectroscopic techniques, such as coherent anti-Stokes Raman scattering spectroscopy and laser induced fluorescence spectroscopy, which have been shown to perform these type of measurements at relevant pressures. However, these techniques are costly and require significant laboratory space and instrumentation to perform. Furthermore, due to the pulsed nature of their light source, these techniques risk ionization of the gas at such low pressures thus perturbing the flow. Our approach is nonintrusive, relatively cheap, spatially compact, and fiber coupled. The following is a description of our approach to develop this instrument.

Optical Design of Fiber Launch System

There are various unique aspects of this optical system that make this research endeavor possible. First and foremost is the design of the multiple-pass cell, discussed later, which greatly enhances the fluence of laser light on the probe volume thereby multiplying the spontaneous Raman signal. Second is the delivery of the laser light through a custom-made optic fiber manufactured by Coastal Connections. The 8-meter long, high power, vacuum optic fiber is capable of transferring the 5-W, 532-nm beam from a Coherent Verdi G Series SLM and couple the light into the multiple-pass cell. The fiber launch system is illustrated in Fig. 1.

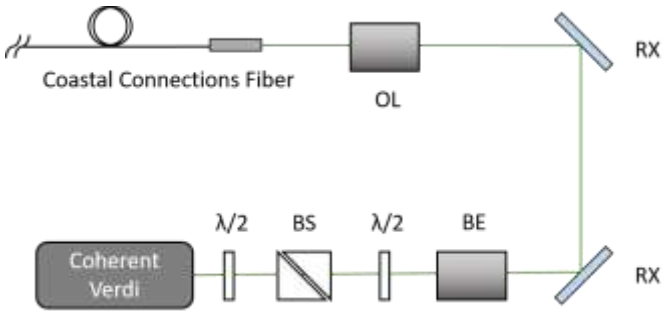

Fig. 1- Fiber launch system used to couple the 5-W, 532-nm beam from a Coherent Verdi G SLM to a high power, vacuum optic fiber by Coastal Connections: half-wave plate (λ/2), polarizing cube beamsplitter (BS), beam expander (BE), objective lens (OL) and mirror (RX).

Particular care must be given to the startup and alignment procedure of the laser to avoid damaging the fiber. The Verdi laser power supply is equipped with a control knob allowing for the modulation of the beam energy output. For optimal performance, the Verdi laser must be powered, set to the maximum beam energy output required and allowed to warm-up for at least hour. The beam energy output must not be changed. Changes to the beam energy output result in thermal changes in the cavity thus provoking beam steering. Maintaining the beam energy output fixed minimizes beam steering. Alignment to the fiber, however, must be performed at low beam energies so as to prevent damaging it. Therefore, at the start of the 1-hour warm-up time, the laser power output is fixed to its maximum of 5-W. The fiber launch system contains a variable attenuator composed of a half-wave plate (Thorlabs, WPH05M-532) and polarizing cube beamsplitter (Thorlabs, GL10-A) to attenuate the beam energy without having to change the energy output.

In order to adequately focus the beam onto the fiber, two conditions must be met: the incident beam must match the numerical aperture of the fiber and the diameter of the incident beam must be smaller than the diameter of the fiber core. For these purposes, a high-power beam expander (Thorlabs, BE02-532), used in reverse, decreases the diameter of the beam from 2.2 mm to approximately 1.1 mm. A high-power objective lens (Thorlabs, LMH-20x-532) then focuses the beam to a nearly diffraction limited diameter. This is much smaller than the 250-μm ferrule of the fiber.

Two mirrors, mounted on kinematic mounts, are used to align the beam onto the fiber. Fine adjustment of the orientation of the fiber with respect to the beam is accomplished by a 4-axis MicroBlock Stage (Thorlabs, MBT402D) with four adjustments: two translation and two rotation. The MicroBlock Stage is mounted on a translation stage (Thorlabs, MBT501) to allow for adjustments in the direction of the optical axis.

The fiber launch system is mounted on a portable cart, as shown in Fig. 2. The cart is a 80/20 T-slot framing system that is 55 inches tall, 36 inches wide and 27 inches deep. The bottom shelf houses the laser power supply, laser chiller and chiller for the Newton EMCCD camera (Andor). The middle shelf houses the Kaiser HOLOSPEC spectrograph and Newton EMCCD camera and its components. The top shelf is fitted with an optical breadboard on which the fiber launch system is fixed. The cart is installed with wheels so that it can be moved as needed and sliding panels to cover and protect the equipment within.

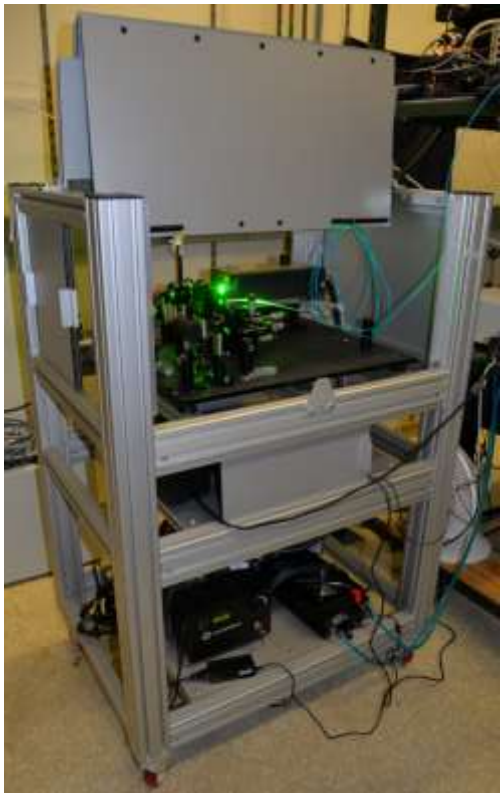

Fig. 2- Portable cart on which fiber launch system is mounted. Bottom and middle shelf house the laser power supply, chiller, spectrograph and EMCCD camera. Top shelf is fitted with optical breadboard and fiber launch system.

On the other end of the fiber, the beam enters the multiple-pass cell and, after nearly 100 passes, exits the cell and is stopped by a beam dump, as illustrated in Fig. 3. The collection of the Raman signal is orthogonal to the multiple-pass cell and is composed primarily of two 100-mm, 2-inch achromatic doublets (Thorlabs, AC508-100-A) that collect the Raman signal and focus it through a 100-µm pinhole. The pinhole was selected so as to limit the dimensions of the probe volume as discussed in the following section. Two additional doublets (Thorlabs, ACA254-050-A and Thorlabs, ACA254-030-532) collect the signal and couple it into a 200-µm fiber. The fiber delivers the collected Raman light to a F/1.8 HoloSpec spectrograph, equipped with a low-frequency grating centered at 532 nm (HSG-532.0, LF) and a Newton EMCCD camera.

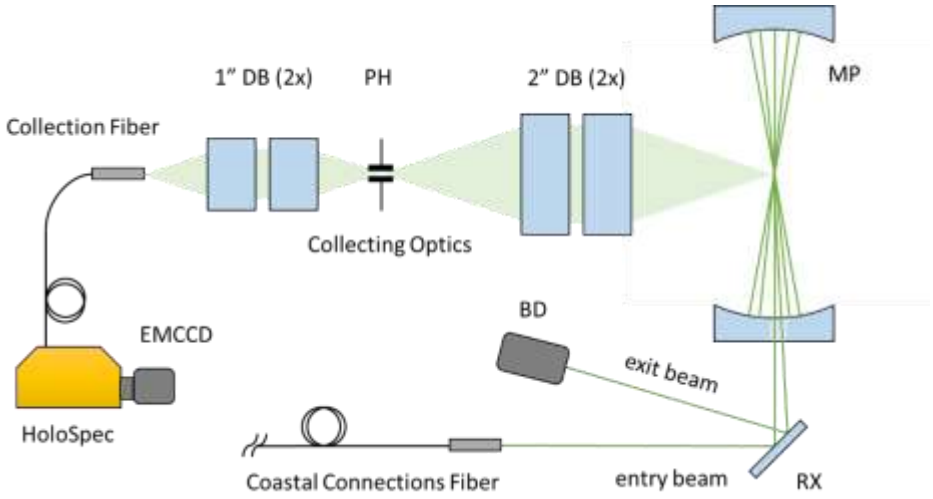

Fig. 3- Raman collection optics and multiple-pass (MP) cell: conflate flange (CF), mirror (RX), doublets (DB), pinhole (PH) and beam dump (BD).

Multiple-pass Cell

The multiple-pass cell was a designed and manufactured by Southwest Sciences Inc. in a similar fashion as those in Ref. [41, 42] with the aim of increasing the laser beam energy density at the center envelope. The concept is straight forward: it is a modified version of a Herriott cell [20, 21]. A beam of light enters the cell of two concentric mirrors through a hole in one of the mirrors, reflects multiple times, refocusing every time, creating an elliptical patters on each mirror, and exits the cell through the same hole it entered. However, designing the multiple-pass cell, such that it performs as described, requires very careful engineering. The design of the multiple-pass cell satisfies the specifications in Tab. 1.

Tab. 1- Specifications for multiple-pass cell.

Item	**Specification**
Number of passes (N)	> 100
Input Wavelength	532 nm
Max Laser Power	5 W
Mirror Spacing	20 cm
Thermally Insensitive	Yes
Vacuum Operation	Yes
Reflectivity	≥ 99.7%
Length of Central Envelope	≤ 1.0 mm (depends on N)
Thickness of Central Envelope	≤ 100 μm (depends on N)

A confocal cavity is created consisting of a pair of spherical mirrors (Rocky Mountain Instrument Co., 2" diameter, 50 mm FL, R> 99.7% at 532 nm) aligned near their concentric limit such that the spacing between the mirrors approaches four times the focal length of the mirrors, as shown in Fig. 4. The software ZEMAX was used to optimize this alignment so as to minimize the beam spot radius at the center envelope of the cell between both mirrors. For this to work, a collimator (Thorlabs, CFC-11X-A) is used to focus the beam from the optical fiber. Separating the mirrors increases the number of passes. The largest number of

passes achievable depends on the stability and optical alignment, especially as the number of passes is increased. For instance, the change in mirror separation to reach 102 passes, from 100 passes, is calculated to be only 8 µm.

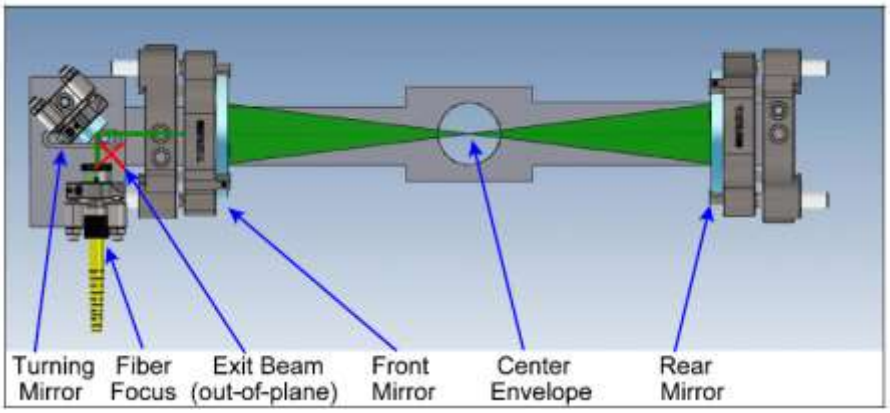

Fig. 4- Diagram of the multiple-pass cell.

At the center envelope, the cross section of the traversing beams create an elliptical pattern like the pattern imprinted on the mirrors when the beam reflects off of them. This is illustrated in Fig. 5. The dimensions of the major and minor axis of the ellipse can be controlled by the alignment of the mirrors and the orientation of the beam entering the cell. The beams do not overlap entirely. However, the minor axis of the ellipse can be minimized so that the traversing beams toward the ends of the elliptical pattern overlap partially. Because of its geometry, increasing the number of passes in the cell also decreases the size of the elliptical envelope of the crossing beams at the center. Continuing to increase the number of passes or decreasing the size of the envelope will ultimately result in the condition in which the beam reflects back unto itself. This must be avoided so as to prevent damaging the fiber.

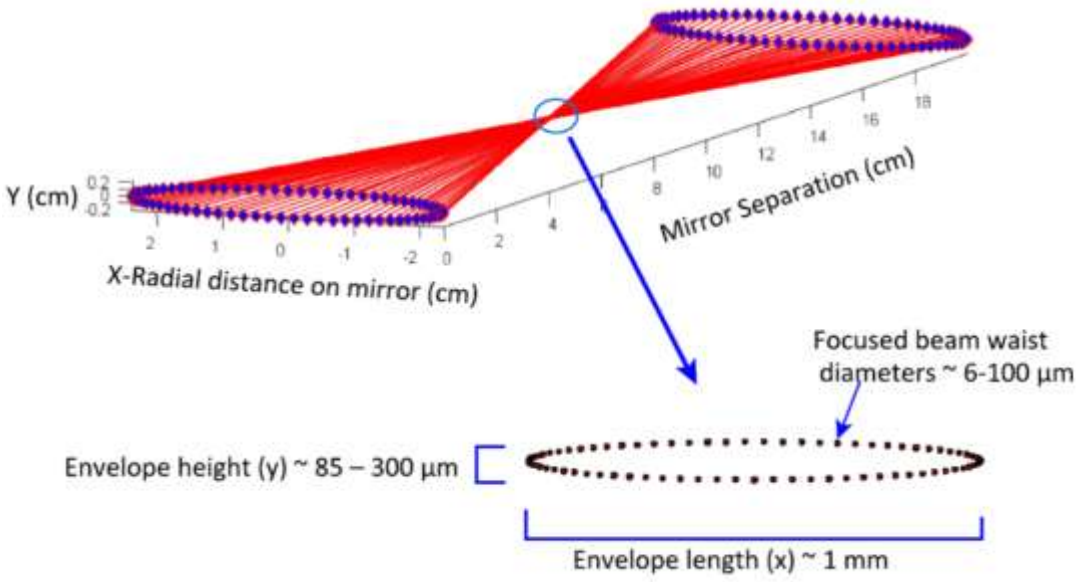

Fig. 5- Diagram of crossing beams and spot pattern at center envelope.

The beam exists the cell through the same hole it entered. However, it exists at a slightly different angle and, as such, can be separated and stopped by a beam dump without damaging the fiber.

Probe Volume

One of the uniquely challenging aspects of this work is the necessity for high spatial resolution (100 µm) at low pressures. As discussed, the scattering signal is greatly amplified by the multiple-pass cell. However, restricting the volume from which the signal is collected, so as to create a small probe volume, also diminishes the gains obtained from the multiple-pass cell.

As shown in Fig. 5 above, the major axis of the center envelope can be as large as 1 mm while the minor axis is in the 85-300 µm range. The reflecting beams overlap at the ends of the elliptical pattern and it is in one of these that a highly spatially resolved Raman signal can be collected. Fig. 6 below illustrates the probe volume carved out by the optical window created by the pinhole in the collecting optics. The pinhole is 100 µm in diameter and serves as the aperture stop for the optical train in the collecting optics. The pinhole is imaged one-to-one by the 100 mm doublets. Therefore, the window of light that is imaged into the 200-µm fiber is also 100 µm in diameter.

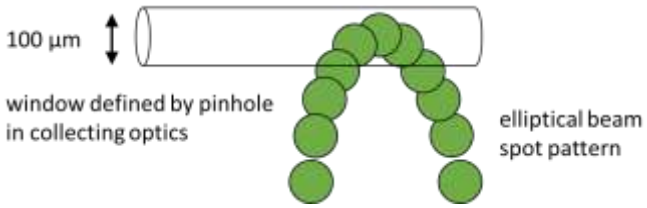

Fig. 6- Illustration of probe volume. Corner elliptical envelope illustrated by green circles. Beam is normal to the page.

The length of the probe volume is defined by the depth of the overlapping beams at the end of the elliptical envelope. It was estimated to be approximately twice the beam waist when the length of the minor axis of the ellipse is minimized. The beam waist at the envelope of the multiple-pass cell was measured at around 86 µm using a knife edge technique in which the distance the knife travels through the cross section of the beam is measured with respect to the beam energy transmitted. Therefore, the length of the probe volume is estimated at approximately 172 µm, or 170 µm to the nearest significant figure.

The approach described above is useful for enhancing the spontaneous Raman and Rayleigh signal scattering from the 100 µm in diameter and 170 µm long probe volume in the multiple-pass cell. In order to study the spontaneous Raman scattering signal, the light collected must be dispersed by a holographic grating in the Kaiser HoloSpec housed in the cart. The Raman spectrum is then collected by a Newton EMCCD camera and a fitting routine, based on a semi-classical approach, can be applied to extract a temperature.

Fitting Routine

A thorough review of semi-classical model and quantum mechanics of the spectroscopy of diatomic molecules can be found in Refs. [3, 43, 44]. Here, we present the equations used to simulate the rotational Raman transitions of a simple diatomic molecule assuming the reader is familiar with the quantized nature of matter at the molecular level and its implications.

The rotational state of a molecule is defined by its rotational quantum number J and its energy is given by

$$E_J = hc[B_0 J(J+1) - D_0 J^2 (J+1)^2] \tag{1}$$

where h is Plank's constant, c is the speed of light, B_0 is the rotational constant at the ground vibrational state, and D_0 is the corresponding centrifugal distortion constant [9]. These constants can be found in Ref. [3] for a variety of molecules, including common diatomic molecules. The Raman shift, from the frequency of the laser light, associated with each rotational transition is given by

$$|\Delta\omega(J)| = (4B_0 - 6D_0)\left(J + \frac{3}{2}\right) - 8D_0(J + \frac{3}{2})^3 \tag{2}$$

The spacing between rotational transitions for diatomic molecules such as N_2 and O_2 are small compared to H_2. Better spectral resolution is achieved when transitions are separately defined and do not overlap. Therefore, in this study, H_2 was used to evaluate the performance of this experimental setup at low pressures.

The intensity of each rotational line is given by

$$I(J) \cong g_n S_J \exp[-\frac{E(J)}{kT}] \tag{3}$$

where g_n is the nuclear degeneracy factor, k is Boltzmann's constant, T is the absolute temperature and

$$S_J = \begin{cases} \frac{(J+1)(J+2)}{2J+3} & \text{Stokes lines} \\ \frac{(J-1)J}{2J-1} & \text{anti-Stokes lines.} \end{cases} \tag{4}$$

Using these equations, a least-square fitting routine can be constructed to fit the spectrum of rotational Raman lines and extract a rotational temperature from the molecule.

MEASUREMENTS IN GAS CELL

A gas cell was constructed from a stainless steel cubic cell with six 2-3/4 conflate flange ports as shown in Fig. 7. A thermocouple and the gas to be studied are introduced from the bottom port. Laser light from the multiple-pass cell is introduced into the gas cell through the ports normal to the page. The cross section of the elliptical pattern at the center envelope that they produce is also illustrated. From the top port, a nichrome wire is introduced to provide a resistive heating mechanism. The wire is connected to a Variac variable transformer utilized to apply a voltage across the wire. The main heating mechanism in the gas cell is convective heating. However, because the wire glows and because the laser light is within a few millimeters of the thermocouple, radiative heating has yield some discrepancy in preliminary measurements. Therefore, the thermocouple was domed with an aluminum foil covering. This removed radiative heating to the thermocouple.

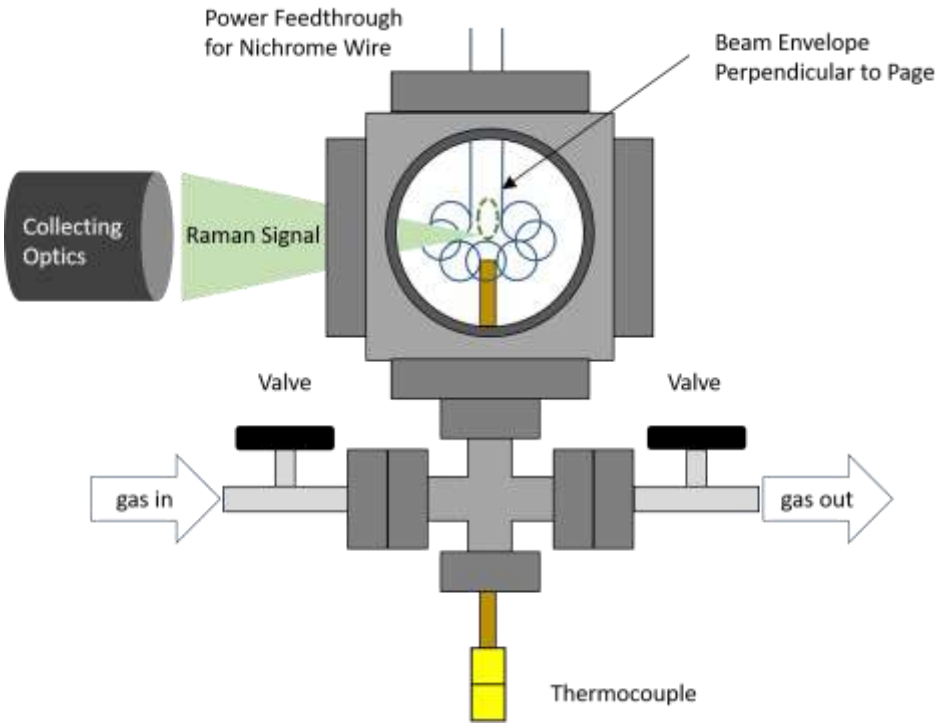

Fig. 7- Gas cell used for validation of H_2 thermometry.

The spontaneous Raman signal is highest in the directions lateral to the gas cube (to the left and right). The collecting optics are illustrated on the left side to capture as much of the Raman signal in that direction. Fig. 8 is a photographic picture of the spectroscopic system and gas cell together. The main components are highlighted: collecting optics, multiple pass cell, and gas cell.

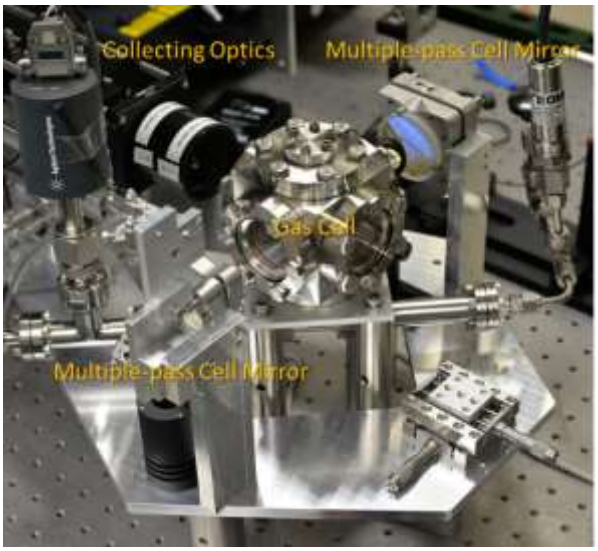

Fig. 8- Multiple-pass cell and collecting optics mounted on diamond plate with gas cell in the center.

Experimental Procedure

At the start of every acquisition, the laser is turned on, set to 5 W and allowed to warm up for at least one hour. Then, the laser power is measured and percent transmittance through the fiber recorded. At 5-W laser power, nearly 60-64 % of the beam power was transmitted in every acquisition. Losses through the fiber launch system are associated with various surface interactions, especially through the variable beam attenuator and at the tip of the fiber.

H_2 is introduced into the cell at the desired pressure and the gas cell is operated as a closed system. Voltage to the nichrome wire is supplied by a Variac variable transformer and the temperature of the gas is allowed to equilibrate for about 10 minutes. This is particularly important at low pressures. Once the temperature of the thermocouple has reached steady state, acquisition of the Raman signal can commence.

In the acquisition process, there are three main parameters that influence the signal-to-noise of the spectra collected: gain on the EMCCD, exposure time, and number of scans recorded. Increasing any of these generally increases signal-to-noise. Increasing the gain, however, is useful up to a certain point after which the noise also scales. In this study, the gain was generally set to 100-150. The exposure time and number of scans required to resolve the spectra strongly depends on the pressure in the gas cell.

RESULTS

The experimental setup and gas cell were first tested at 155 Torr. Fig. 9 (a) illustrates a sample spectrum of the measured Raman signal and the fitted spectrum at 155 Torr. A temperature of 561 K was extracted at a Variac variable transformer voltage of 10 V. The thermocouple in this case measured a temperature nearly 20 K lower, as shown in Fig. 9 (b). This difference is minimized at lower temperatures. This is because as the temperature of the resistive wire increases so does the thermal gradient between the wire and the walls of the gas cell. The walls of the gas cell are exposed to the environment and are not heated by any secondary means other than convection from the gas within. The thermocouple and probe volume are approximately 3-5 millimeters apart and this gradient could explain the 20 K discrepancy at the highest temperature probed.

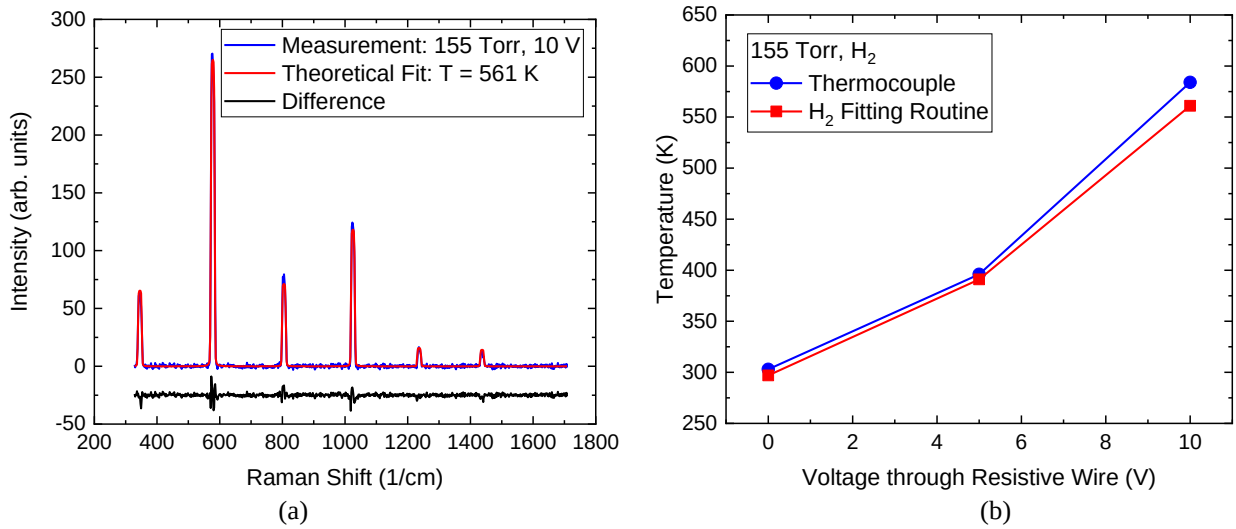

Fig. 9- (a) Sample H_2 spectra measured at 155 Torr, 10 V and (b) temperature profiles in gas cell.

A 100 µm slit was used in the HoloSpec spectrograph to resolve the H_2 rotational Raman lines in Fig. 9 above. However, a slit is not necessary. The rotational Raman lines for H_2 are separately resolved even without a slit, as shown in Fig. 10 below, and the relative intensities of each transition is not affected. This is useful because the characteristic shape of rotational lines with a slit < 100 µm are similar to the noise at low pressures. This means that rotational lines are better resolved without a slit at pressures where the Raman signal is very low and long exposure times are necessary. Furthermore, the slit does not define the dimensions of the probe volume. Therefore, studies <1 Torr were performed without a slit.

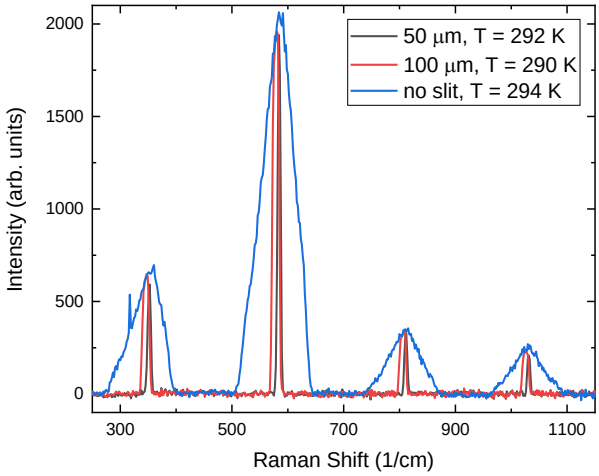

Fig. 10- Comparison of H_2 rotational transitions with spectrograph slit size.

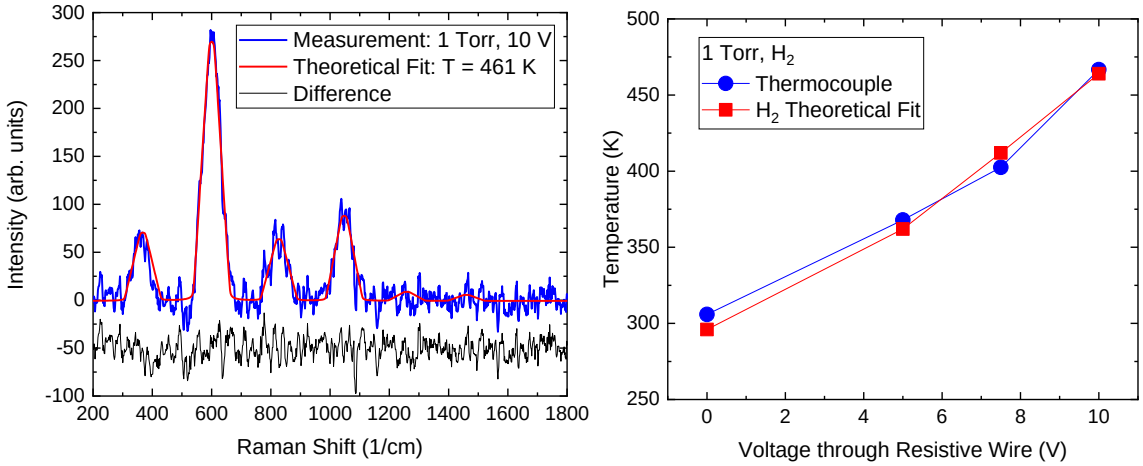

(a) (b)

Fig. 11- (a) Sample H_2 spectra measured at 1000 mTorr, 10 V and (b) theoretical fits temperature profile in gas cell. Camera settings: 90-s exposure time, 30 frames averaged, 100 gain.

The objective of this proposal was to develop the diagnostic tools to perform highly spatially resolved measurements of Raman and Rayleigh spectroscopy to study the thermodynamics of non-equilibrium flows at low pressures (< 1 Torr). The measurements in Fig. 9 were performed to quickly

illustrate the performance of the diagnostic instrument and computational model for spontaneous Raman spectroscopy for rotational H_2 lines. Figs. 11 and 12 illustrate results at much lower pressures than Fig. 9, 1000 mTorr and 500 mTorr respectively.

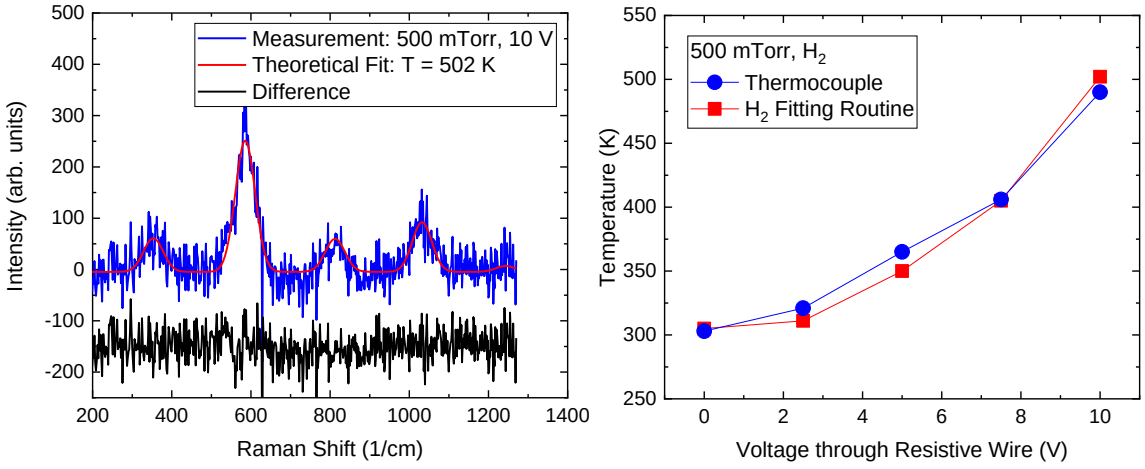

(a) (b)

Fig. 12- (a) Sample H_2 spectra measured at 500 mTorr, 10 V and (b) theoretical fits temperature profile in gas cell. Camera settings: 60-s exposure time, 30 frames averaged, 100 gain.

The spectra in Figs. 11 and 12 are well resolved. Each rotational H_2 line is spectrally separate. The broadening of each line, as a result of the missing slit in the Holospec spectrograph, helps to resolve each line above the noise. The temperatures extracted from the spectral fits agree well with the thermocouple measurements, within error. Because of the low pressures, the collisional rate with the cold walls of the cell are much less than at higher pressures. This means that the temperature gradient near the probe volume and the tip of the thermocouple is reduced. As a result, there is no apparent bias in either temperature profile as the voltage in the Variac variable transformer increases.

CONCLUSIONS

Various aspects of the proposal herein have been accomplished. Primarily, we have developed a spectroscopic instrument capable of performing highly spatially resolved (100 µm diameter, 170 µm length) spontaneous Raman spectroscopy measurements of rotational H_2 lines at pressures relevant to satellite propulsion (< 1 Torr). Proof-of-principle experiments testing the performance of the spectroscopic instrument show that temperatures extracted from fits are close to thermocouple measurements, thus validating the spectroscopic instrument developed in this work. The instrument described herein is not only relatively compact and inexpensive, but also portable and ready for Raman thermometry of H_2 of low pressure, non-equilibrium flows. This is particularly useful in probing the plume of a micro-jet for satellite propulsion.

FUTURE WORK

Several tasks remain, however, to fulfill every item proposed. If calibrated correctly, Raman spectroscopy may be used to extract a number density of the gas in question. This aspect of the spectroscopic instrument has yet to be examined. Furthermore, the Rayleigh component of the proposal, to

measure velocity and translational temperature, has not been explored. However, most of the necessary instrumentation for the filtered Rayleigh scattering work has already been put together. The primary missing component is the introduction of an iodine cell in the path of the signal. Various aspects of this missing part have been evaluated and are soon to be accomplished.

ACKNOWLEDGEMENT

We would like to acknowledge Joel Silver, PhD from Southwest Sciences Inc. for his consultation and for producing the multiple-pass cell used in this work. Additionally, the authors are grateful to Mr. Adam Burkley for participating in some of the data acquisition presented in this research endeavour during his summer internship at the US Naval Research Laboratory.

REFERENCES

[1] C. V. Raman and K. S. Krishnan, "A New Type of Secondary Radiation," *Nature,* vol. 121, pp. 501-502, 1928.

[2] H. A. Szymanski, Raman Spectroscopy: Theory and Practice, New York: Plenum Press, 1967.

[3] N. M. Laurendeau, Statistical Thermodynamics, Cambridge: Cambridge University Press, 2005.

[4] D. R. Beattie and M. A. Cappelli, "Raman Scattering Measurements of Molecular Hydrogen in a Low-density, Arc-heated Plasma," *Applied Physics B,* pp. 419-427, 2000.

[5] I. D. Boyd, D. R. Beattie and M. A. Cappelli, "Numerial and Experimental Investigations of Low-density Supersonic Jets of Hydrogen," *Journal of Fluid Mechanics,* pp. 41-67, 1994.

[6] W. G. Breiland, M. E. Coltrin and P. Ho, "Comparisons Between a Gas-phase Model of Silane Chemical Vapor Deposition and Laser-diagnostic Measurements," *Journal of Applied Physics,* vol. 59, pp. 3267-3273, 1986.

[7] R. B. Miles, W. R. Lempert and J. N. Forkey, "Laser Rayleigh Scattering," *Measurement Science and Technology,* vol. 12, pp. R33-R51, 2001.

[8] J. A. Sutton and R. A. Patton, "Improvements in Filtered Rayleigh Scattering Measurements Using Fabry-Perot Etalons for Spectral Filtering of Pulsed, 532-nm Nd:YAG Output," *Applied Physics B,* vol. 116, pp. 681-698, 2014.

[9] U. Doll, E. Burow, G. Stockhausen and C. Willert, "Methods to Improve Pressure, Temperature and Velocity Accuracies of Filtered Rayleigh Scattering Measurements in Gaseous Flows," *Measurement Science and Technology,* vol. 27, 2016.

[10] U. Doll, G. Stockhausen and C. Willert, "Pressure, Temperature, and Three-component Velocity Fields by Filtered Rayleigh Scattering Velocimetry," *Optics Letters,* vol. 42, no. 19, pp. 3773-3776, 2017.

[11] J. A. Wehrmeyer, T. S. Cheng and R. W. Pitz, "Raman Scattering Measurements in Flames Using a Tunable KrF Excimer Laser," *Applied Optics,* vol. 31, no. 10, 1992.

[12] G. Grunefeld, V. Beushausen, P. Andresen and W. Hentschel, "Spatially Resolved Raman Scatetring for Multi-Species and Temperature Analysis in Technically Applied Combustion Systems: Spray Flame and Four-Cylinder In-line Engine," *Applied Physics B,* vol. 58, pp. 333-342, 1994.

[13] A. V. Sepman, V. V. Toro, A. V. Mokhob and H. B. Levinsky, "Determination of Temperature and Concentrations of Main Components in Flames by Fitting Measured Raman Spectra," *Applied Physics B,* vol. 112, pp. 35-47, 2013.

[14] J. Kojima and Q. V. Nguyen, "Measurement and Simulation of Spontaneous Raman Scattering in High-Pressure Fuel-rich H2-air Flames," *Measurement Science and Technology,* vol. 15, pp. 565-580, 2004.

[15] J. Kojima and Q. V. Nguyen, "Single-shot Rotational Raman Thermometry for Turbulent Flames Using a Low-resolution Bandwidth Technique," *Measurement Science and Technology,* vol. 19, 2008.

[16] X. Li., Y. Xia, L. Zhan and J. Huang, "Near-confocal Cavity-enhanced Raman Spectroscopy for Multitrace-gas Detection," *Optics Letters,* vol. 33, no. 18, 2008.

[17] A. J. Friss, C. M. Limbach and A. P. Yalin, "Cavity-enhanced Rotational Raman Scattering in Gases Using a 20 mW Near-infrared Fiber Laser," *Optics Letters,* vol. 41, no. 14, 2016.

[18] J. Thorstensen, K. H. Haugholt, A. Ferber, K. A. H. Bakke and J. Tschudi, "Low-cost Resonant Cavity Raman Gas Probe for Multi-gas Detection," *Journal of European Optical Society Rap. Public.,* vol. 9, 2014.

[19] S. Ohara, S. Yamaguchi, M. Endo, K. Nanri and T. Fujioka, "Performance Characteristics of Power Build-up Cavity for Raman Spectroscopic Measurement," *Optical Review,* vol. 10, no. 5, pp. 342-345, 2003.

[20] R. A. Hill and D. L. Hartley, "Focused, Multiple-pass Cell for Raman Scattering," *Applied Optics,* pp. 186-192, 1974.

[21] W. R. Trutna and R. L. Byer, "Multiple-pass Raman Gain Cell," *Applied Optics,* pp. 301-312, 1980.

[22] G. C. Stutzin, A. T. Young, A. S. Schlachter, K. N. Leung and W. B. Kunkel, "In Situ Measurements of Rovibrational Populations of H2 Ground Electronic state in a Plasma by VUV Laser Absorption," *Chemical Physics Letters,* vol. 155, no. 4, 1989.

[23] Y. Takama and K. Suzuki, "Spectroscopic Observation of Translationa-rotational Nonequilibrium in Low-density Hydrogen Plasma Flow," *Journal of Thermophysics and Heat Transfer,* vol. 23, no. 3, 2009.

[24] H. H. Reising, U. KC, N. T. Clemens and P. L. Varghese, "Measurement of Mixing-induced Thermal Non-equilibrium in a Supersonic Shear Layer Using Spontaneous Raman Scattering," *Physics of Fluids,* vol. 29, 2017.

[25] R. G. Seasholtz and A. E. Buggele, "Improvement in Suppression of Pulsed Nd:YAG Laser Light With Iodine Absorption Cells for Filtered Rayleigh Scattering Measurements," National Aeronautics and Space Administration, Washington, DC, 1997.

[26] I. Binietoglou, P. Giampouras and L. Belegante, "Linear Approximation of Rayleigh-Brillouin Scattering Spectra," *Applied Optics,* vol. 55, no. 27, 2016.

[27] B. Witchas, Z. Gu and W. Ubachs, "Temperature Retrieval From Rayleigh-Brillouin Scattering Profiles Measured in Air," *Optical Society of America,* vol. 22, no. 24, 2014.

[28] T. Wu, J. Shang, C. Yang, X. Zhang, H. Yu, Q. Mao, X. He and Z. Chen, "Spontaneous Rayleigh-Brillouin Scattering Spectral Analysis Based on the Wiener Filter," *AIP Advances,* vol. 8, 2018.

[29] A. Mielke, K. A. Elam and C. Sun, "Rayleigh Scattering Diagnostics for Measurements of Temperature, Velocity, and Density Fluctuation Spectra," in *44th AIAA Aerospace Sciences Meeting and Exhibit*, Reno, 2006.

[30] A. F. Mielke, K. A. Elam and C. J. Sung, "Development of a Rayleigh Scattering Diagnostic for Time-resolved Gas Flow Velocity, Temperature and Density Measurements in Aerodynamic Test Facilities," in *IEEE,* 2007.

[31] A. F. Mielke, K. A. Elam and C. J. Sung, "Time-resolved Rayleigh Scattering Measurements in Hot Gas Flows," in *46th AIAA Aerospace Sciences Meeting and Exhibit*, Reno, 2008.

[32] A. Mielke and K. A. Elam, "Dynamics Measurements of Temperature, Velocity, and Density in Hot Jets Using Rayleigh Scattering," in *14th International Symposium on Applications of Laser Techniques to Fluid Mechanics*, Lisbon, 2008.

[33] I. D. Boyd, D. B. VanGilder and E. J. Beiting, "Computational and Experimental Investigations of Rarefied Flows in Small Nozzles," *AIAA Journal,* vol. 34, no. 11, 1996.

[34] E. J. Beiting, "Coherent Anti-Stokes Raman Scattering Velocity and Translational Temperature Measurements in Resistojets," *Applied Optics,* vol. 36, no. 15, 1997.

[35] L. T. Williams, M. S. McDonald and M. F. Osborn, "Performance Characterization of a Low Reynolds Number Micro-Nozzle Flow," in *AIAA*, 2015.

[36] R. H. Lee, T. C. Lilly, E. P. Muntz and A. D. Ketsdever, "Free Molecule Micro-resistojet: Nanosatellite Propulsion," in *Air Force Research Laboratory*, Edwards AFB, 2005.

[37] Z. Ahmed, S. F. Gimelshein and A. D. Ketsdever, "Numerical Analysis of Free-molecule Microresistorjet Performance," *Journal of Propulsion and Power*, vol. 22, no. 4, 2006.

[38] M. M. Hussaini and J. J. Korte, "Investigation of Low-Reynolds-Number Rocket Nozzle Design Using PNS-Based Optimization Procedure," NASA Technical Memorandum, Hampton, 1996.

[39] T. D. Holman and M. F. Osborn, "Numerical Optimization of Micro-nozzle Geometries for Low Reynolds Number Resistojets," in *AIAA*, 2015.

[40] M. F. Osborn, T. D. Homan, D. A. Rosenberg and S. G. Tuttle, "Overocming Low Nozzle Efficiency: A Test-Correlated Numerical Investigation of Low Reynolds Number Micro-Nozzle Flow," in *AIAA*, 2015.

[41] K. C. Utsav, J. A. Silver, D. C. Hovde and P. L. Varghese, "Improved Multiple-pass Spectrometer," *Applied Optics,* vol. 50, no. 24, pp. 4805-4816, 2011.

[42] K. C. Utsav and P. L. Varghese, "Accurate Temperature Measurements in Flames with High Spatial Resolution Using Stokes Raman Scattering from Nitrogen in a Multiple-pass Cell," *Applied Optics,* pp. 5007-5021, 2013.

[43] A. C. Eckbreth, Laser Diagnostics for Combustion Temperature and Species, CRC Press, 1996.

[44] L. C. Hoskins, "Pure Rotational Raman Spectroscopy of Diatomic Molecules," *Journal of Chemical Education*, pp. 568-572, 1975.

[45] U. KC, J. A. Silver, D. C. Hovde and P. L. Varghese, "Improved Multiple-pass Raman Spectrometer," *Applied Optics,* pp. 4805-4816, 2011.

[46] L. Xiao-Yun, X. Yu-Xing, H. Ju-Ming and Z. Li, "Diagnosis of Multiple Gases Separated from Transformer Oil Using Cavity-Enhanced Raman Spectroscopy," *Chinese Physical Society,* pp. 3326-3329, 2008.

[47] X. Li, Y. Xia and L. H. J. Zhan, "Near-confocal Cavity-enhanced Raman Spectroscopy for Mutitrace-gas Detection," *Optics Letters,* pp. 2143-2145, 2008.

[48] D. Kirk Viers and G. M. Rosenblatt, "Raman Line Positions in Molecular Hydrogen: H2, HD, HT, D2, DT, and T2," *Journal of Molecular Spectroscopy,* pp. 401-419, 1987.

[49] A. V. Sepman, V. V. Toro, A. V. Mokhov and H. B. Levinsky, "Determination of Temperature and Concentration in Flames by Fitting Measured Raman Spectra," *Applied Physics B,* pp. 35-47, 2013.

[50] D. Herriott, H. Kogelnik and R. Kompfner, "Off-axis paths in Spherical Mirror Interferometers," *Applied Optics,* vol. 3, pp. 523-526, 1964.

[51] Z. Gu and W. Ubachs, "A Systematic Study of Rayleigh-Brillouin Scattering in Air, N2, and O2 Gases," *The Journal of Chemical Physics,* vol. 141, 2014.

[52] G. Magnotti and R. S. Barlow, "Dual-resolution Raman Spectroscopy for Measurements of Temperature and Twelve Species in Hydrocarbon-air Flames," *Proceedings of the Combustion Institute,* vol. 36, pp. 4477-4485, 2017.

[53] L. Xiao-Yun, X. Yu-Xing, H. Ju-Ming and Z. Li, "Diagnosis of Multiple Gases Separated from Transofrmer Oil Using Cavity-Enhanced Raman Spectroscopy," *Chinese Physics Letters,* vol. 25, no. 9, 2008.

[54] G. J. Williams, J. J. Kojima, L. A. Arrington, M. C. Deans, B. D. Reed, M. I. Kinzbach and C. H. McLean, "Plume Characterization of a Laboratory Model 22 N GPIM Thruster Via High-frequency Raman Spectroscopy," in *AIAA*, Orlando, 2015.

[55] D. A. Roseberg, B. A. Williams, S. G. Tuttle and M. F. Osborn, "Optical Measurements of Density and Species Concentration in a Low Reynolds Number Micro-nozzle Flow," in *AIAA*, Kissimmee, 2015.

[56] J. Bouwmeester and J. Guo, "Survey of Worldwide Pico- and Nanosatellite Missions, Distributions and Subsystem Technology," *Acta Astronautica,* vol. 67, pp. 854-862, 2010.

[57] W. A. de Groot and F. J. Zupanc, "Laser Rayleigh and Raman Diagnostics for Small Hydrogen/Oxygen Rockets," in *Proceedings of SPIE,* 1993.

[58] A. Cervone, A. Mancas and B. Zandbergen, "Conceptual Design of a Low-pressure Micro-resistojet Based on a Sublimating Solid Propellant," *Acta Astronautica,* vol. 108, pp. 30-39, 2015.